Catalysis
Science &
Technology

rsc.li/catalysis

Volume 7
Number 2
21 January 2017
Pages 313-534

ISSN 2044-4761

ROYAL SOCIETY OF CHEMISTRY

PAPER
Chaoqiu Chen, Yong Qin et al.
Highly dispersed Pt nanoparticles supported on carbon nanotubes produced by atomic layer deposition for hydrogen generation from hydrolysis of ammonia borane

ROYAL SOCIETY OF CHEMISTRY

rsc.li/catalysis

ARTICLE

The Role of Photocatalysts in Radical Chains of Homolytic Aromatic Substitutions, Radical Addition to Olefins, and Nucleophilic Radical Substitution Mechanisms

Damian E. Yerien,[a] Sebastián Barata-Vallejo,*[a,b] Erwin W. Mora Flores,[a] Al Postigo*[a]

Photoinitiated perfluorobutylation reactions of 2-anisidine **1**, propenyloxybenzene **2**, and 2-mercaptoethanol **3** have been carried out employing commercially available n-C_4F_9-I as source of $^{\bullet}C_4F_9$ radicals under three different photocatalysts (PCs) absorbing in the violet ($Ir[(dF(CF_3)ppy]_2(dtbbpy)^+$ (PC-1)), green (Rose Bengal (PC-2)) and red (Zinc phthalocyanine PhZn (PC-3)) regions of the electromagnetic spectrum, in order to explore the quantum yields and radical chain lengths for each type of transformation and photoinitiated system. For substrates **1**-**3** and their different types of reactions, the comparative study between PCs seeks to establish the extent to which regioproducts, yields, and mechanistic proposals are influenced by the intervention of each PC. The different overall quantum yields and chain lengths obtained for each type of reaction under each PC are a direct consequence of the efficiency of the photoinitiation events, primary radical production, propagation and termination steps. This will have important implications in the understanding and representations of the mechanisms postulated, in terms of closed and open catalytic cycles. One strategy we apply to uncover radical propagating chains in our mechanisms is to explore photocatalysts that operate in oxidative and reductive quenching manners for each type of transformations.

Introduction

An increasing number of chemical transformations can be accomplished through the aid of visible light and the use of (organo)metallic photocatalysts[1] that gather light in the form of energy to generate reactive species that enable various transformations towards synthetic targets needed in different fields. Mechanistic details regarding photoinitiated organic reactions are acknowledging new insights into the processes involved, providing a thorough comprehension of the scope and role of photocatalysts in organic reactions.[2-5] This new focus on photocatalysis, i.e.: conjoining synthetic and mechanistic detailed studies of photocatalytic reactions, departs from the conventional mere synthetic approach utilized in the early applications of organic photocatalysis.[2]

Within the field of visible light photocatalytic transformations,[6] late-stage fluoroalkylation reactions (introduction of fluorinated groups in the last stages of synthetic protocols) have played a relevant role, as fluoroalkyl group substitutions bring positive impacts on the physical properties of organic compounds, including solubility, metabolic stability, and lipophilicity, which are properties of considerable importance in pharmaceutical, agrochemical, and materials science when designing targets of biological importance and building blocks.

A distinction should be made between the terms 'photocatalytic process' *vs* 'photoinitiated or photoinduced processes'. For self-propagating radical processes, where the photocatalyst is responsible for the initiation event that produces the first radical to enter the chain loop, the chemistry should be discussed as photoinitiation,[5d] and not as a photocatalytic reaction. If the PC intervenes in other mechanistic cycles, such as in the propagation, then, a photocatalytic process is operating.

One area of constant disagreement in photocatalysis is whether photoredox reactions involve radical chain mechanisms. In Figures 1**A** and 1**B** the photoredox perfluoroalkylation reactions of an olefin under an oxidative and reductive quenching cycles are illustrated.

a.-Universidad de Buenos Aires, Facultad de Farmacia y Bioquímica-Junín 954 CP 1113- Buenos Aires-Argentina. apostigo@ffyb.uba.ar; sbaratavallejo@ffyb.uba.ar
b.- Istituto per la Sintesi Organica e la Fotoreattività (ISOF), Consiglio Nazionale delle Ricerche (CNR), Bologna, Italy
Electronic Supplementary Information (ESI) available: [details of any supplementary information available should be included here]. See DOI: 10.1039/x0xx00000x
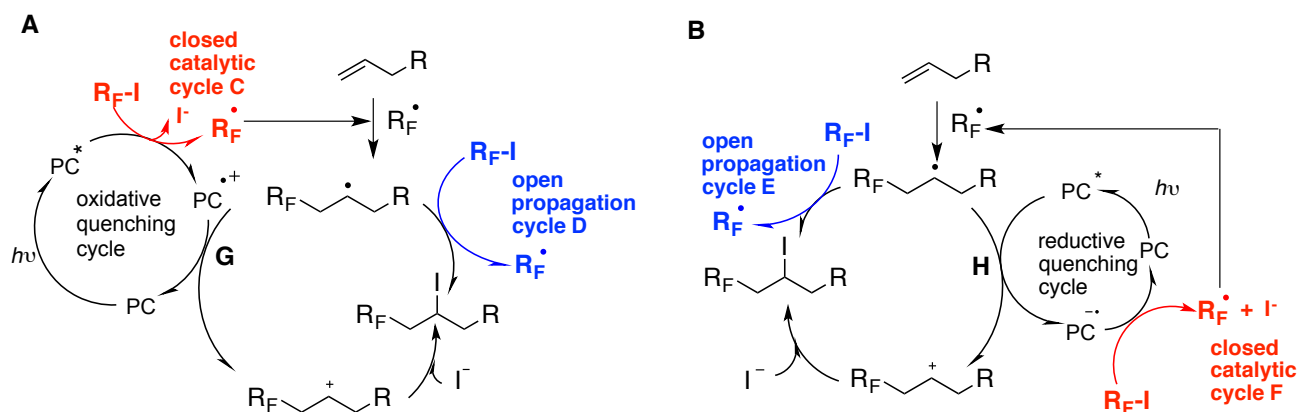
ARTICLE

Fig. 1. A: Coupled- closed and open- photoinitiated cycles for the oxidatively-induced photoredox process. **B**: Coupled- closed and open-photoinitiated cycles for the reductively-induced photoredox perfluoroalkylation of olefin

Both Figures 1**A** and 1**B** summarize *closed* (red) and *open* (blue) photoinitiated oxidative and reductive quenching cycles, respectively. However different in the photoinitiation these two mechanisms (Figures 1**A** and 1**B**) may seem, the same propagation cycles (cycles **D** and **E**, Figure 1**A**, and 1**B**, respectively) are described.

Scenarios of both processes (i.e.: oxidative[7-9] and reductive[10,11]) are present in the literature. Radical chains in photoinitiated reactions[12-15] are currently postulated in the literature as well as closed catalytic loops.[16]

The exploration of chain lengths in photocatalytic reactions is then an assertive tool to bring to light the actual photocatalytic / photoinitiated process.

The necessity for constant illumination in a photocatalytic/photoinitiated reaction is interpreted as very short chain processes or no chain at all. In the literature, this is currently shown as photocatalytic experiments where periods of irradiation times are intercalated with dark intervals, and observing a build-up of product only when the reaction is under constant illumination, and a plateau during dark periods.[18,19] However, typical radical chain processes normally take place on the second or sub-second time scale;[20a-c] and so, the observation that product conversion is discontinued under absence of light could also be in agreement with chain processes that cease faster than the timescale employed in the analytical measurement.[2] In this regard, the group of Scaiano[21] came up with a set of experiments to determine radical chains in very fast photocatalyzed reactions, through the rotating sector experiment using intermittent LEDs.

In this paper, we show that under the same radical propagation steps proposed in a given catalytic mechanism (such as cycles **D** or **E**, Fig. 1**A** and 1**B**, respectively) when different PCs are employed, lower than-unity overall quantum yields can still disguise radical propagation events operating in a photoinitiated mechanism eclipsed by inefficiencies of the initiation or termination events. Thus for a given reaction, the employment of different photocatalysts operating under distinctive reductive and oxidative quenching manners (different PCs) will help uncover the presence of radical chains in propagation steps revealed by some PCs and masked by the use of others. These studies will make use of quantum yields, luminescence measurements and computational results to study chain processes in photoinitiated perfluoroalkylation reactions. For that purpose, three ordinary classes of organic processes will be studied: homolytic aromatic substitutions (HAS), radical addition to olefins (atom transfer radical addition, ATRA), and radical-thiolate coupling reactions. The investigation will make use of three different types of photocatalysts absorbing in the violet, green and red regions of the electromagnetic spectrum, respectively. Correlations between radical chain lengths, photon and Gibbs energies and redox properties under each photocatalyst will be presented in order to help draw more accurate mechanistic proposals.

Results and Discussion

The photoinitiated perfluorobutylation reactions of 2-anisidine (2-methoxyaniline) **1**, propenyloxybenzene **2**, and 2-mercaptoethanol **3** have been carried out employing commercially available n-C$_4$F$_9$-I as source of C$_4$F$_9$ radicals under three different photocatalysts, i.e.: Ir[(dF(CF$_3$)ppy)$_2$(dtbbpy)$^+$ (PC-1), Rose Bengal (4,5,6,7-Tetrachloro-3',6'-dihydroxy-2',4',5',7'-tetraiodo-3H-spiro[isobenzofuran-1,9'-xanthen]-3-
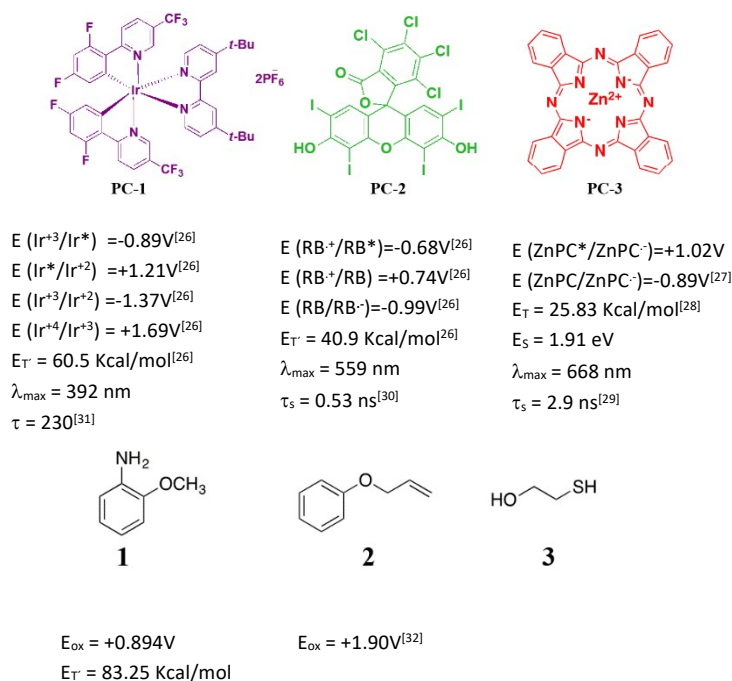
one (PC-2), and Zinc phthalocyanine ZnPh (PC-3). The reaction types that are going to be studied / exposed under the three PCs are Homolytic Aromatic Substitution HAS (substrate **1**), Atom Transfer Radical Addition ATRA (substrate **2**), and aliphatic radical-anion coupling substitution S_RN (substrate **3**). This is the first study aimed at evaluating the scope of perfluoroalkylation reactions of arenes, olefins and thiols employing three different photocatalysts which absorb light in three different regions of the visible electromagnetic spectra,

using sources of light from violet LEDs (392 nm), green LEDs (525 nm) and red LEDs (657 nm), comparing the product quantum yields, radical chain lengths, regioselectivity and yields. The optimization of reaction-conditions for the reactions studied are detailed in the ESI (Table S1-S3).[23-25] Table 1 summarizes the reaction conditions employed under the three types of photocatalysts for substrates **1-3**.

Table 1. Reaction conditions for the perfluorobutylation of substrates **1-3** (0.2 mmol) with n-C_4F_9-I (3 equiv) employing different PCs under irradiation in indicated Ar-deoxygenated solvent (3 mL), in the presence of additives at room temperature, under constant stirring.

entry	system	Photocatalyst	$\lambda_{máx}$ (nm)[a]	solvent	Additive (equiv)
1	1	$Ir[(dF(CF_3)ppy]_2(dtbbpy)^+$ (**PC-1**)	392	CH_3CN	Cs_2CO_3 (1.5)
2	2	Rose Bengal (**PC-2**)	525	CH_3CN	Cs_2CO_3 (1.5)
3	3	Zinc phthalocyanine (**PC-3**)	657	CH_3CN:DMF	Ascorbic acid (1.5) Collidine (1.5)

a.- λ_{max} of irradiation (LED) employed

PC-1

E (Ir^{+3}/Ir^*) = -0.89V[26]
E (Ir^*/Ir^{+2}) = +1.21V[26]
E (Ir^{+3}/Ir^{+2}) = -1.37V[26]
E (Ir^{+4}/Ir^{+3}) = +1.69V[26]
$E_{T'}$ = 60.5 Kcal/mol[26]
λ_{max} = 392 nm
τ = 230[31]

PC-2

E ($RB^{·+}/RB^*$) = -0.68V[26]
E ($RB^{·+}/RB$) = +0.74V[26]
E ($RB/RB^{·-}$) = -0.99V[26]
$E_{T'}$ = 40.9 Kcal/mol[26]
λ_{max} = 559 nm
τ_s = 0.53 ns[30]

PC-3

E ($ZnPC^*/ZnPC^-$) = +1.02V
E ($ZnPC/ZnPC^-$) = -0.89V[27]
E_T = 25.83 Kcal/mol[28]
E_S = 1.91 eV
λ_{max} = 668 nm
τ_s = 2.9 ns[29]

1

E_{ox} = +0.894V
$E_{T'}$ = 83.25 Kcal/mol

2

E_{ox} = +1.90V[32]

3

## Homolytic aromatic substitutions of electron-rich arenes with PCs-1-3

Nöel and colleagues[33] have accomplished the Eosin-Y-photocatalyzed perfluoroalkylation of (hetero)aromatic substrates employing perfluoroalkyl iodides R_F-I and N,N,N',N'-tetramethylethylene diamine (TMEDA) as base. Our group and others`[34] have shown that efficient Electron Donor Acceptor EDA complexes[34b] formed between R_F-I and organic bases such as TMEDA can accomplish perfluoroalkylation reactions of (hetero)arenes, sulfides, and carbon-carbon multiple bonds by visible light activation in the absence of a photocatalyst. Based on our previous results on the photoinitiated perfluoroalkylation of (hetero)aromatic compounds with Rose Bengal[23], and with zinc phthalocyanine[24] as photocatalysts we

decided to employ inorganic bases such as Cs_2CO_3 and collidinium ascorbate, respectively, in order to minimize EDA complexes formation between R_F-I and organic bases.

The first reaction type investigated under the three different photoinitiated systems (systems 1-3, Table 1) is the HAS of 2-anisidine **1** with the perfluorobutyl group. Optimization of the reaction conditions for the three photoinitiated systems is displayed in Tables S1-S3. The stoichiometry employed was chosen to maximize the formation of the *para*-substituted isomer. Table 2 illustrates the mass balance and the product ratios of the perfluorobutylation products obtained. Mass balance in all cases is very good, being the regioselectivity ratios encountered under the three photoinitiated systems very similar. Under prolonged photoreaction times (i.e.: 20 hrs), two substitution products are formed in very high yield (90-94%); i.e.: 2-methoxy-4-(perfluorobutyl)aniline **1A**, and 2-methoxy-

4,6-bis(perfluorobutyl)aniline **1B**, being **1A** the major product under the three photoinitiated systems (PCs-1-3). However, **1B** is not a primary reaction product, and is formed at the expense of 2-methoxy-6-perfluorobutylaniline **1C** (not shown) (ratio **1A**:**1C** *ca.* 1:0.1).

Table 2. Reaction products form the perfluorobutylation of substrate **1** (0.2 mmol) with *n*-C$_4$F$_9$-I (3 equiv) employing different PCs (PC-1-3) in indicated Ar-deoxygenated solvent (3 mL), in the presence of additives irradiating at room temperature for 20 hrs under constant stirring.
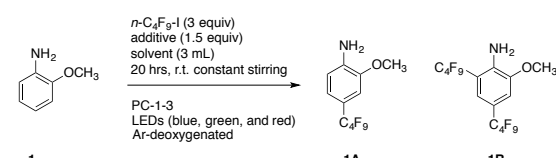
| entry	system	$\lambda_{máx}$ (nm)[a]	Mass balance,[b] %	1A:1B Product ratio, %
1	1	392[c]	94	80:20
2	2	525[d]	97	83:17
3	3	657[e]	98	82:18

a.- λ_{max} of irradiation (LED) employed $\pm$ 2 nm. b.- ca. 100% mass balance was obtained, indicating that substrate converts only to products in yields reported, with the remainder of the mass being unreactive substrate. c.- calibrated violet LEDs, 3 Watts. d.- calibrated green LEDs, 3 Watts. e.- calibrated red LEDs, 3 Watts

Previous kinetic studies[23] indicate that the *para*-substituted product is formed first, followed by an *ortho*-substituted product. Disubstituted product **1B** is formed at the expense of the build-up of the *ortho*-substituted product. Notably, the three PCs can accomplish the HAS reaction of **1** with C$_4$F$_9$ radicals with excellent mass balances. At low substrate conversion (5-7%) only product **1A** is observed (*vide infra*) and very minor amounts of 2-methoxy-6-perfluorobutylaniline **1C** start to grow.

From a quick inspection of Table 2, the selection of PC-3 under the red- light irradiation source provides comparable yields of products **1A-B** than the other visible-light excited PCs, enabling the employment of aryl substrates with large UV spectral bathochromic shifts, facilitating the perfluoroalkylation of highly-conjugated activated aromatic targets that otherwise could absorb in the violet or even green regions of the electromagnetic spectrum competing with the PCs absorption.[24,35]

Mechanistic evidence, such as the quenching of the photoinitiated reactions (systems 1-3) with TEMPO (Scheme 1**A**) and 1-methyl-1-phenyl-ethylene (product **4A**, Scheme 1**B**), suggests the presence of radicals. The photoinitiated reactions of **1** with Ir[(dF(CF$_3$)ppy]$_2$(dtbbpy)$^+$ (PC-1) and Zn-phthalocyanine (PC-3) as photocatalysts are suppressed in the presence of 1,4-dinitrobenzene (Scheme 1**C**), purporting the presence of an ET process involving radical anions. This quenching is a result of being 1,4-dinitrobenzene a more suitable electron scavenger, accepting an electron either from Ir(II) or ZnPh radical anion (which prevents the transfer of the odd electron to n-C$_4$F$_9$-I). On the other hand, the photoinitiated reaction of **1** with RB (PC-2) as PC is not suppressed with 1,4-dinitrobenzene (Scheme 1**D**), purporting to the absence of an acting reducing species better than RB*. The fluorescence spectra of Ir[(dF(CF$_3$)ppy]$_2$(dtbbpy)$^+$ are quenched upon addition of a DMF solution of Cs$_2$CO$_3$ (ET from CO$_3^{2-}$ to PC-1*, as in Figure S2A), whereas

the fluorescence spectra of RB are suppressed upon addition of *n*-C$_4$F$_9$-I, which is evidence of an ET pathway between excited RB* and *n*-C$_4$F$_9$-I (Figure S2B). On the other hand, the fluorescence spectra of Zn-phthalocyanine PC are suppressed when adding 2,4,6-collidinium ascorbate (Figure S2C). On the contrary, fluorescence spectra of either Ir[(dF(CF$_3$)ppy]$_2$(dtbbpy)$^+$ (PC-1) or Zn-phthalocyanine (PC-3) are not modified upon addition of *n*-C$_4$F$_9$-I (Figure S3 for PC-1), which means that no ET takes place between PC* and C$_4$F$_9$-I. Therefore, PC-1 (i.e.: Ir(III)) would not oxidize to Ir(IV) transferring an electron to C$_4$F$_9$-I in an oxidative quenching manner, neither PC-3 would oxidize to Zn-Phthalocyanine radical cation and reduce C$_4$F$_9$-I to C$_4$F$_9$ radicals in an ET process.
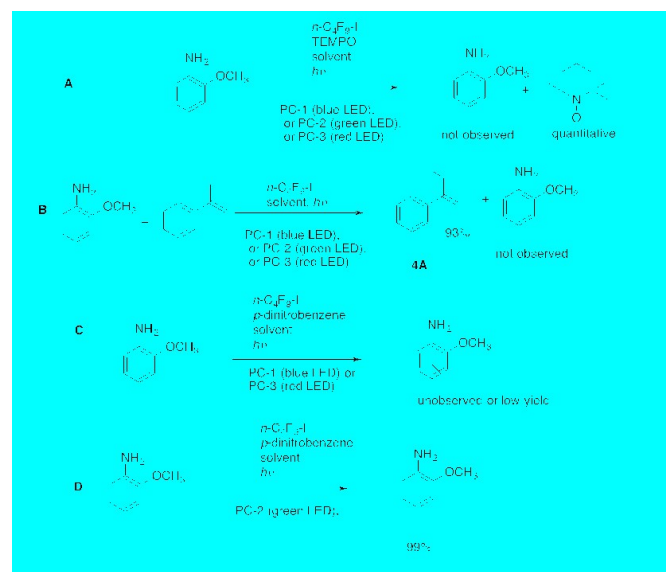
Scheme 1. Mechanistic probe experiments for the perfluorobutylation of **1** under three photoinitiated systems. **A**.-Use of TEMPO under PCs-1-3. **B**.-Use of 1-methyl-1-phenyl ethelyne as probe under PCs-1-3. **C**.-Use of p-dinitrobenzene under PC-1 and PC-3. **D**.-Use of p-dinitrobenzene under PC-2

The proposed cycles for the production of C$_4$F$_9$ radicals with PCs-1-3 are shown in Figures 2**A-C**. The Gibbs energy differences for the production of •C$_4$F$_9$ radicals with the three PCs are calculated according to the Rehm Weller equation 1.

$$\Delta G = E^o_{red} (D/D^+) - E^o_{red} (A/A^-) - E^*(0,0) - w \quad (1)$$

Where E^o_{red} (D/D$^+$) is the reduction potential of the species that is being oxidized, E^o_{red} (A/A$^-$) the reduction potential of the species which is reduced, E^{o,o} the excited state triplet energy, and *w* the coulombic term.

In Figure 2**A**, the use of PC-1 (i.e.: Ir[(dF(CF$_3$)ppy]$_2$(dtbbpy)$^+$) in a reductive quenching cycle affords C$_4$F$_9$ radicals from the reduction of *n*-C$_4$F$_9$-I by ground state Ir(II) (reductive ET). The ΔG_{ET} is calculated to be exergonic by -0.1 V.
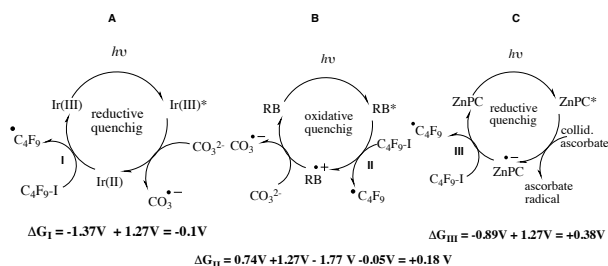
Fig. 2. A: Proposed photoinitiated cycle (Ir[(dF(CF$_3$)ppy]$_2$(dtbbpy)$^+$) for the initiation (production of $^\bullet$C$_4$F$_9$ radicals) and calculation of the Gibbs energy involved in the process. **B**: Proposed photoinitiated cycle (Rose Bengal) for the production of $^\bullet$C$_4$F$_9$ radicals and calculation of the Gibbs energy involved in the process. **C**: idem for Zn-phthalocyanine photocatalyst

Metal-organo-photoredox catalysts[3] such as PC-1, can act in both oxidative and reductive quenching cycles. However, as fluorescence of PC-1* does not seem to be suppressed by n-C$_4$F$_9$-I (Figure S3), ET oxidation of Ir(III)* to Ir(IV) and concomitant reduction of n-C$_4$F$_9$-I to $^\bullet$C$_4$F$_9$ radicals is precluded, ruling out an oxidative quenching cycle with PC-1. Instead, the fluorescence of PC-1* is readily quenched by addition of Cs$_2$CO$_3$ DMF solution (Figure S2A), purporting that an ET reduction takes place between PC-1* and Cs$_2$CO$_3$, generating a carbonate radical anion (ECO$_3^{\bullet-}$/CO$_3^{2-}$ = +1.23 +/–0.15 V). The ΔG$_{ET}$ for this process is calculated to be slightly exergonic by -0.08V (see ESI, Section IX.2).[36]

In Figure 2**B**, the use of PC-2 (Rose Bengal) in an oxidative quenching cycle affords $^\bullet$C$_4$F$_9$ radicals from the reduction of n-C$_4$F$_9$-I by excited state RB reductive ET, supported by Stern Volmer quenching experiments, where the luminescence of RB* is effectively quenched by addition of n-C$_4$F$_9$-I (Figure S2B). The ΔG$_{ET}$ is calculated to be +0.18 V, which is somewhat endergonic. According to Figure 2**B**, PC-2 is postulated to be regenerated from PC$^{\bullet+}$ by the carbonate ion and affords the carbonate radical anion. Although this latter process is somewhat endergonic (calculated ΔG$_{ET}$ = +0.49 V, see ESI, Section IX.2), would generate an excellent oxidant species, the carbonate radical anion, which in turn could further oxidize the resulting radical adduct of the arene to a Wheland intermediate (calculated ΔG$_{ET}$ = -0.76 V, see ESI, Section IX.2). We will next show (*vide infra* in the postulated mechanism) that this is not the main route to re-establish the thermoneutral PC-2.

The excited state of PC-3* is quenched by 2,4,6-collidinium ascorbate, according to Stern Volmer quenching experiments (Figure S2C), supporting the proposal of Figure 2**C**. The use of PC-3 (Zn-phthalocyanine) in a reductive quenching cycle affords C$_4$F$_9$ radicals from the reduction of n-C$_4$F$_9$-I by the radical anion of PC-3 reductive ET. The ΔG$_{ET}$ is calculated to be endergonic by +0.38 V. These results are summarized in Table 3 (see also Table S12)

Table 3. Difference in Gibbs energies for the ET step producing C$_4$F$_9$ radicals, according to Figure 2

entry	system	E$_{PC/PC\cdot-}$ (V)	E$_{PC\cdot+/PC}$ (V)	ET (eV)	ΔG$_{ET}$ (eV)
1	1	-1.37	+1.69	2.62	**-0.1**
2	2	-0.99	+0.74	1.77	**+0.18**
3	3	-0.89	-	1.12	**+0.38**

Although this reduction process from PC-3$^{\bullet-}$ to n-C$_4$F$_9$I (Figure 2**C**) is a thermodynamically unfavourable ET[37] (from the reduced

photocatalyst to C$_4$F$_9$I (about +0.38 V)), 2,4,6-collidinium ascorbate could aid in the activation of the carbon iodine (C–I) bond to overcome this endergonic event, acting as a Lewis acid.[38] Also, Shibata and colleagues[35] in the subphthalocyanine- photocatalyzed trifluoromethylation of olefins under red light found an endergonic ΔG$_{ET}$ process by more than +0.5 V, from the excited photocatalyst to CF$_3$-I; the reduction of the CF$_3$-I by PC* still taking place.[35] As a matter of fact, the R$_F$-I bond has been shown to be weakened under photoinitiation in the presence of chloride ions,[39] amines,[40] and carbonyl compounds (esters).[41,42] In a recent report by some of us,[24] theoretical calculations were carried out revealing that ΔG from PC-3$^{\bullet-}$ to n-C$_4$F$_9$I is indeed an exergonic event with a value of -12.11 Kcal/mol, suggesting the role of PC-3$^{\bullet-}$ in the production of $^\bullet$C$_4$F$_9$ radicals, according to Figure 2**C**.

Yoon and colleagues[19a] have demonstrated that in Ru-photocatalyzed Diels Alder radical cation reactions and the enone [2 + 2] radical anion cycloaddition reactions, radical chain mechanism intervene, and a conjecture was raised that in most other photocatalyzed transformations this latter scenario can also be the case. In the same lines, Teders, Glorius and collaborators[19b] have also shown that in the Ir-photocatalyzed functionalization of benzotriazole substrates photocatalytic-initiated chain mechanisms prevail as indicated by determination of the reaction quantum yields and Stern–Volmer analyses. We undertook the task of assessing the presence of chain propagation mechanisms in HAS reactions of activated arenes with the perfluoroalkyl group under different photoinitiated systems (systems **I-III**, as in Table 2).

Quantum yields are characteristic of photoreactions under a specific set of conditions and can vary significantly as a function of wavelength and the nature of the photocatalyst.

To launch our investigations on chain propagation in the radical photocatalytic (photoinitiated) perfluoroalkylation of substrate **1**, and to support or exclude a chain propagation cycle, we determined the quantum yield measurements under the three photoinitiated systems, utilizing calibrated violet, green, and red LEDs (with emission maxima at 392 nm, 525 nm, and 657 nm, respectively). Absolute measurement of incident photon flux was achieved by means of calibrated photodiodes which are widely used for the detection of electromagnetic radiation in the ultraviolet, visible, and infrared range.[43] Silicon photodiodes for light power measurement with resolution of 1 nW were employed. For LEDs with emission maxima at 392 nm a calibrated UV-enhanced silicon sensor for 250-400 nm range (Coherent OP-2 UV) was used; and for LEDs with emission maxima at 525 nm and 657 nm a calibrated silicon sensor for 400-1064 nm (Coherent OP-2 VIS) was employed. In all cases, measurements of the light that passed through the bottom of the vial were performed at the mouth of the vial (vial walls were covered with a bright white optical film to ensure total light reflection, Figures S4-S6).The incident photon flux measured by photodiodes was corroborated by chemical actinometry (potassium ferrioxalate for λ_{max} = 392 nm for PC-1, and λ_{max} = 525 nm for PC-2, and Reinecke salt, for λ_{max} = 657 nm, for PC-3, ESI).[43,44] For the 392 nm LED (3 Watts, which radiant power ET is 8 mWatt), the photon flux is calculated to be 1.5787 x 10^{16} photons/sec. For the 525 nm LED (radiant power ET = 10 mWatt), the value obtained is 2.6429 x 10^{16} photons/sec., and for the 657 nm LED (ET = 16 mWatt), the photon flux is 5.2916 x 10^{16} photons/sec. The calculations of photon flux obtained with calibrated diodes and that obtained from chemical actinometry is illustrated in ESI, Section VIIa-b.

Substrate **1**, and additives are transparent at all PCs maxima absorption wavelengths or diode emissions so we could make the

ARTICLE

limiting assumption that the incident photon flux is absorbed solely by the photocatalyst (absorption fraction ≥ 0.99). After irradiation, the number of moles of product **1A** formed is quantified by ^{1}H and ^{19}F NMR spectroscopy using an internal standard (benzotrifluoride, see Table S9, ESI, for number of moles calculation for each PC). An average of three determinations were taken. The cumulative quantum yield for product formation from the perfluoroalkylation of **1** can be calculated by dividing the moles of **1A** formed by the einsteins of photons consumed (eq 2).

The einsteins of light absorbed (mol x s^{-1}) equal the mole of photons per seconds times the irradiation time (s). From these data, we calculate a quantum yield value of $\Phi = 3.81\pm0.16$ for PC-1, 0.51 ± 0.03 for PC-2, and 0.17 ± 0.01, for PC-3 (Table 4A), respectively.

$$\phi = \frac{\text{moles of product formed}}{\text{einsteins of light absorbed}} \quad (2)$$

This calculation does not consider the involvement of any other photoinitiated processes that do not lead to product. For example, the photoexcited PC* catalyst could relax to the ground state through either radiative or vibrational pathways without undergoing ET processes; the reduced photocatalyst PC$^{\bullet-}$ and the oxidized arene could also recombine to regenerate PC and neutral arene via back electron transfer. The possibility of energy transfer (EnT) between PC* and **1**, which would deactivate the excited state of the PC, should be ruled out, according to the values of triplet energies of **1** and those of the PCs (footnote of Table 1).

This, nonetheless, would lead to a reduction of the numerator of eq 2 without affecting the denominator. Consequently, the actual chain length could be higher than the measured quantum yield *(vide infra)*. Therefore, although the observation of a quantum yield much greater than unity provides confirmation of a chain nature of the reaction, the actual length of the chains could be substantially higher than the determined quantum yield. On the contrary, the observation of a quantum yield lower than unity does not necessarily reflect on a lack of any propagation chain (or generation of the primary radical species by an alternate secondary event), as significant initial loss of energy can be provoked by non-productive processes.[13]

According to the procedure of Yoon and colleagues,[19a] the quenching fraction Q is calculated according to eq 3:

$$Q = \frac{k_{q\,(\textbf{PC})}[\textbf{Q}]}{\tau^{-1} + k_{q(\textbf{PC})}[\textbf{Q}]} = \frac{K_{SV}[\textbf{Q}]}{1 + K_{SV}[\textbf{Q}]} \quad (3)$$

Where K_{SV} is the Stern-Volmer coefficient which is determined by Stern Volmer rate quenching experiments (Figure S2-S3). Applying eq. 3, the Q values are calculated and illustrated in Table 4A. The chain length (**L**) is approximated by dividing the measured quantum yield ϕ by the quenching fraction Q. This ratio (i.e.: ϕ/Q) is governed by both ϕ and Q values, and could result in large L numbers should the quenching fraction be small. A more precise measurement of L could be estimated as the ratio between the propagation rate and the addition of the rates of all termination steps. If the photoinitiator is involved in a termination step (as in step **G**, Figure 1**A**, and step **H**, Figure 1**B**), then the photoinitiator (i.e.: photocatalyst) should be playing a role in the actual chain length.

Table 4A. Measurements of quantum yields (ϕ) quenching fractions (Q) and chain lengths (L) for the photoinitiated production of product **1A** from the perfluorobutylation reaction of **1** under three photocatalysts

entry	system	K_{SV} (M^{-1})	ϕ^a	Q^b	L
1	1	402	$3.81^c \pm 0.16$	0.979	3.9
2	2	4.3	$0.51^d \pm 0.03$	0.340	1.5
3	3	162	$0.17^e \pm 0.01$	0.951	0.18

a.- electronic actinometry employed. Calculation using equation 2. Moles of product formed calculated employing an internal standard by NMR integration (^{19}F and ^{1}H NMR spectroscopy experiments). Table S9, ESI. b.- using equation 3. c.- measured at λ = 392 nm, high power LED, 3 Watt, radiant power ET = 8mWatt. d.- measured at λ = 525 nm, high power LED, 3 Watt, radiant power ET = 10 mWatt. e.- measured at λ = 657 nm, high power LED, 3 Watt, radiant power ET = 16 mWatt

As triplet energy of the PCs (see footnote Table 1 for value of triplet energy ET of PCs and **1**), are lower than that of substrate **1**, an energy transfer process (EnT) should be ruled out in systems 1-3.[45a,b] As observed form Table 4A, quantum yields for the perfluorobutylation reaction of **1** do not reveal, *a priori*, the presence of significant propagation events (entries 1-3, column 5, Table 4A). In Scheme 2**A** (reductive quenching cycles), $^{\bullet}$C$_4$F$_9$ radicals are produced from the ET reduction of C$_4$F$_9$-I by PCs radical anions (i.e.: Ir(II) and PCZn$^{\bullet-}$, step II) , whereas in Scheme 2**B** (oxidative quenching cycle) $^{\bullet}$C$_4$F$_9$ radicals are produced from the ET reduction by excited PC* (RB*), step IV. A more realistic measurement of the efficiency of step II (Scheme 2**A**), could be supplied by dynamic quenching of fluorescence experiments.[45c]

The calculated quenching fractions Q for PC-1 and PC-3 do not directly reflect on the initial production of $^{\bullet}$C$_4$F$_9$ radicals (as in step II, Scheme 2A) but the formation of the reduced species from PC-1$^{\bullet-}$ and PC-3$^{\bullet-}$ (step I, Scheme 2A) instead. Consequently, the percentage of the excited state fractions of the PC-1 and PC-3 that gives rise to $^{\bullet}$C$_4$F$_9$ radicals is not given by the Q value, and the actual quenching fractions of the excited states of PC-1* and PC-3* that produce C$_4$F$_9$ radicals could be smaller than those calculated from equation 3. This would result in longer chain lengths than shown from Table 4A for PC-1. On the other hand, for PC-3, the endergonic nature of step II, Scheme 2A (($\Delta G_{II\,(PC-3)}$ = +0.38 eV, vide supra, Figure 2**C**) accounts for the low cumulative quantum yield observed with PC-3 (i.e.: 0.17).

In Scheme S2 (section VIII, ESI) another mechanistic proposal is illustrated employing PC-1, where the radical anion of the substitution product, intermediate **C**, is formed through base-induced deprotonation of intermediate **A**. In this proposal, the open catalytic cycle is controlled by the ET reduction from **C** to C$_4$F$_9$-I, which produces more C$_4$F$_9$ radicals that propagate the chain (step III, Scheme 2S). However, in previous publications we have demonstrated through Linear Free Energy Relationships (Hammet plots) that the actual nature of the intermediate in the radical reactions of perfluoroalkylation of aniline derivatives is the Wheland intermediate **B** (Scheme 2, *vide infra*) rather the radical anion of the substitution product (intermediate C, Scheme 2S, ESI).[23] Therefore, Scheme 2**A** is more representative of the actual mechanism for the photoinitiated perfluoroalkylation of aniline derivatives with PC-1.

The photoinitiated reaction of substrate **1** employing PC-2 (i.e.: Rose Bengal) does not involve either an apparent significant chain length (i.e.: 1.5); however, a lower-than-unity quantum yield (i.e.: 0.51) is found. The calculated quenching fraction Q is small (i.e.: 0.34)

which directly reflects on the efficiency of $^\bullet C_4F_9$ radicals formation. This means that only 34% of the excited state of PC-2 is involved in producing $^\bullet C_4F_9$ radicals. The remainder 66% of the excited PC-2 is likely involved in other processes such as radiative or internal conversion.

As observed from Scheme 2, the propagation cycles (open catalytic cycles), are proposed to be identical for both oxidative and reductive quenching events (*c.f.* steps **III**, and **V**, Scheme 2**A** and 2**B**, respectively). In the postulated propagation steps (**III**, or **V**, Scheme 2) the oxidation of adduct **A** by C_4F_9-I is the same regardless of the PC. This does not mean equal propagation chains for the three photocatalysts. In fact, the chains are influenced by the nature of the PC, and the competing efficiency of initiation and termination processes.

For PC-1 and PC-3, the calculated quenching fractions are similarly high (>95%). We discussed that these Q values obtained (Q_{PC-1} and Q_{PC-3}) do not represent the quenching fractions of the excited states of the PCs that give rise to the primary radical species ($^\bullet C_4F_9$ radical) that kicks in the loop, as PC-1 and PC-3 excited states are not suppressed by addition of C_4F_9-I (*vide supra*), but by addition of Cs_2CO_3 and collidinium ascorbate solutions, respectively. Therefore, the calculated chain lengths L resulting from dividing the quantum yield ϕ by the photocatalyst quenching fraction Q are lower limit measurements to determine L for PC-1 and PC-3.

However, even if a measure of the efficiency of step **II** (production of $^\bullet C_4F_9$ radicals, Scheme 2**A**) could be determined, the efficiency of the termination step (as the quantum yield of termination) would have to be considered. Therefore, the lower quantum yields observed for systems II and III (PC-2, and PC-3) are a result of poor initiation or termination events for these two PCs. The inefficiency of the initiation for PC-3 (production of the first C_4F_9 radical event) has been disclosed by the endergonic ΔG_{ET} calculated for this process (Table 3, entry 3). Despite that for PC-2 the calculated ΔG for the initiation process is not as endergonic as that for PC-3 (Table 3, entry 2), the quenching fraction is low (Table 4, entry 2), contributing to a global inefficient photoreaction. For PC-2, oxidative quenching cycle, (Scheme 2**B**), radical adduct **A** could be oxidized to Wheland intermediate **B** by the radical cation of PC-2$^{\bullet+}$ (RB$^{\bullet+}$), whose $E_{ox\ PC-2.+}$ = +0.74 V[26], as depicted in step **VI**, Scheme 2B (see also Section IX.2.-, ESI). Computationally- obtained data (Table 4B, entry 2 and ESI, Table S13) support that the bimolecular chain-terminating event is substantially more exergonic than the essentially thermoneutral chain-propagation event (Table 4B, entry 2, and Table S13, ESI). This is rather surprising as two short lived intermediates (**A** and RB$^{\bullet+}$) could be responsible for the

production of the Wheland complex **B**. These data support the contribution of a closed loop in the photoreaction with PC-2. Also, oxidation of radical adduct **A** by carbonate radical anion can also be proposed, as the carbonate radical anion is an excellent oxidant species (and the process has a calculated ΔG_{ET} = -0.76 V, see ESI, section IX.2). However, given that formation of $CO_3^{\bullet-}$ was calculated to be an endergonic event from the radical cation of Rose Bengal (ΔG_{ET} = +0.49 V, see ESI, Section IX.2), regeneration of the active PC-2 is made by radical adduct **A** rather than $CO_3^{\bullet-}$, as the former has a large exergonic Gibbs energy (Table 4B, entry 2). The oxidation of radical adduct **A** to Wheland intermediate **B** is also possible by PC-1* and PC-3* (Scheme 2**A**, path **I**), assuming an E_{ox} for intermediate **A** *ca.* 0.47 V vs. SCE for secondary alkyl radical[46], and $E_{red\ PC-1*}$ = +1.21 V and $E_{red\ PC-3*}$ = +1.02 V vs. SCE [27a], oxidation events for **A** by PCs* should be favourable (ESI, section IX.2.). This would support the role of closed loops in the mechanism, or that both closed and open loops are operative. Computational data (see Table S13, ESI and Table 4B, entry 1) support that radical intermediate **A** is more likely to be oxidized to Wheland intermediate **B** in the closed cycles (in red) by PC-3* rather than by n-C_4F_9-I in an open propagation event (in blue). Although these calculations afford more exergonic events for the oxidation of **A** by PC-Zn* (entry 1, Table 4B) rather than by C_4F_9-I (entries 1,3, Table 4B, respectively), step **III** (Scheme 2A) is the one accounting for a chain propagation event. Also, as referred to before, we surmise that the calculated chain lengths L for PC-1 are underestimated (*vide supra*) which could only mean that the chain length is even longer than that calculated by L.

Table 4B. Simulated ΔG, ΔH, ΔS at the B3LYP/LANL2DZ theory level at 298 K

entry	Reaction	ΔG^a	ΔH^a	ΔS^a
1[b]		-26.8	-28	-3.8
2[c]		-52.3	-53.8	-4.9
3[d]		+1.2	+9.6	+28.2
4[e]		-12.1	-3.2	+30

a.-in Kcal/mol. b.-see step I, Scheme 2**A**. c.- see step VII, Scheme 2**B**. d.-see step III, Scheme 2**A** and step V, Scheme 2**B**. e.- see step II, Scheme 2**A**

In Scheme 2**B** (oxidative quenching cycle), we could argue that both open and closed catalytic cycles shown in paths **IV** (in red) and path **V** (in blue), respectively, are playing roles for $^\bullet C_4F_9$ radical production.

ARTICLE
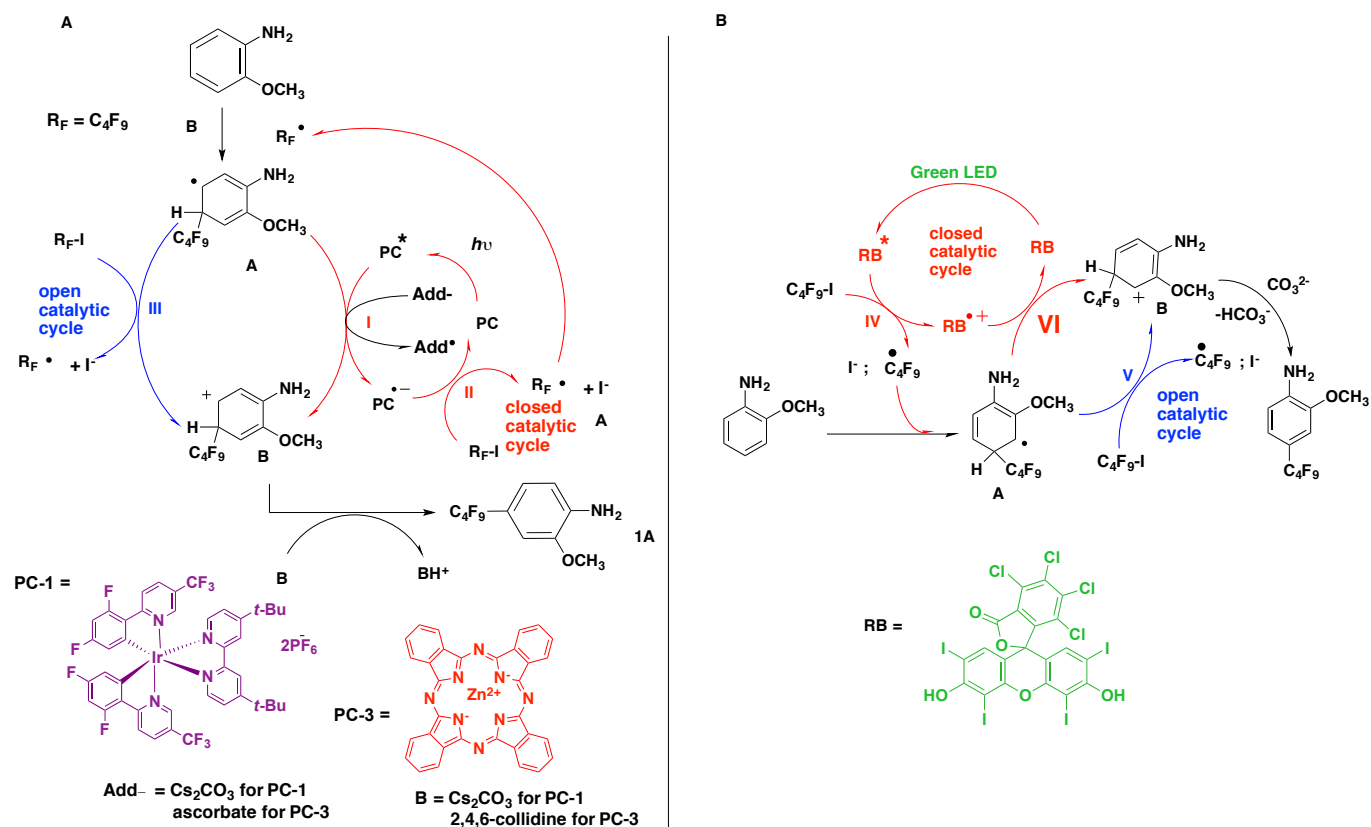
Scheme 2. **A**: Proposed reaction pathway for the photoinitiated (PC-1 and PC-3) perfluorobutylation of arenes. **B**: Proposed reaction pathway for the photoinitiated (PC-2) perfluorobutylation of arenes

Summary for the HAS reaction of 2-anisidine with •C_4F_9 radicals:

For the HAS reaction of **1** with •C_4F_9 radicals under the three PCs, quantum yields vary significantly as a function of wavelength as observed from Table 4A. Particularly in this case, a decrease in the photon energy of the incident light translates into a reduction of the quantum   yield.

   Chain length can be considered as resulting from the ratio between the rate of chain propagation divided by the sum of the rates of all chain termination events. As PCs 1-3 are proposed to be involved in chain termination events (step **I**, Scheme 2**A** for PC-1 and PC-3, and step **VI**, Scheme 2**B**, for PC-2, respectively), then, the PCs should have some bearing on the lengths of chains. Therefore, varying the structure of the photocatalyst can change its contribution to the rate of chain termination and thus to chain length. Therefore, the measured chain length (as $L = \phi / Q$) could not be a proper indication of the efficiency of the propagation, either because the primary process for the quenching fraction Q (of the excited state of the PC) is not the production of the initiating •C_4F_9 radical or else not all the parameters that affect the initiation and termination events are cancelled out in the oversimplified ratio $\phi / Q = L$. As a matter of fact, Pitre, Scaiano and colleagues[21] have suggested that quantum yields lower than unity do not necessarily reflect on lack of chains.

   In the case of PC-2, given the somewhat inefficient initiation process (as revealed by low Q_{RB}), then, the efficiency of step **VI** in regenerating PC-2 (Scheme 2B) might be playing a substantial role. In fact, according to our calculations, the oxidation of the radical adduct intermediate **A** by RB$^{\bullet+}$ (radical cation of Rose Bengal) (step **VI**, Scheme 2**B**) is a highly exergonic event (calculated as -52.3 Kcal/mol, entry 2, Table 4B). This step (i.e. **VI**, Scheme 2**B**), which affords the

Wheland intermediate, derives to product after deprotonation. Therefore, the regeneration of the active form of the PC-2 from its radical cation should be described in mechanistic proposals such as that shown in step **VI**, Scheme 2**B**, rather than that postulated in Figure 2**B** by carbonate ion. This latter has been mistakenly postulated before in proposed mechanisms.[23]

Being the photonic process different for each of the three photocatalysts (translated into different quantum yields for each PCs) and being the global quantum yield a product combination of the initiation, propagation and termination quantum yields of the overall process, the calculated chain length L (associated with the propagation quantum yield) derived from quantum yield and the quenching fraction (equation 3), is biased by the efficiency of the photoinitiation (primary production of $^•C_4F_9$ radicals) and termination processes and cannot be taken as an accurate measure of the efficiency of the propagation.

Figure S7 (see ESI) illustrates a graphical representation of the quantum yields ϕ, chain lengths L, and quenching fraction Q for the photoinitiated production of 1**A** under photocatalysts PCs-1-3. A corollary of the processes shown could emphasize that a seemingly lower-than-unity quantum yield (i.e.: for PC-3) would not necessarily mean lack of chain, but the inefficiency of other processes involved. Also, that both open and closed catalytic loops are operating simultaneously in photoinitiated perfluoroalkylation reactions of arenes. As observed from Table 4A, both quantum yield, and apparent chain lengths decrease as the photon energy of the irradiation source decrease. However, the light-harvesting efficiency within each PC is intimately related to the efficiency of the photoinitiation and termination events.

Photoinitiated radical addition to olefins

The second reaction type investigated was the perfluorobutyl radical addition to an olefinic system (an atom-transfer radical addition reaction, ATRA). The substrate employed was propenyloxybenzene **2**. Table 5 illustrates the mass balance and the perfluorobutylation product obtained, under the three photoinitiated systems (irradiating at three different wavelengths). Optimization of reaction conditions for the three photoinitiated systems can be found in Tables S1-S3.

Table 5. Photoreaction conditions form the perfluorobutylation of substrate **2** (0.2 mmol) with n-C_4F_9-I (3 equiv) employing different photocatalysts PCs (PC-1-3) in indicated Ar-deoxygenated solvent (3 mL), with additives at room temperature.
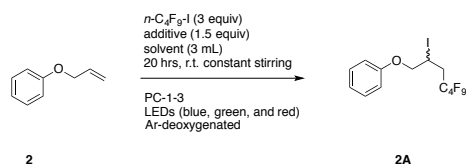
entry	system	PC (mol%)	$\lambda_{máx}$ (nm)	Mass balance,[a] %
1	1	PC-1 (0.5)	392 [b]	99
2	2	PC-2 (0.5)	525 [c]	98
3	3	PC-3 (0.5)	657 [d]	99

a.- Substrate conversion after 20h-irradiation. b.-violet LEDs, 3 Watt, E_T = 8 mWatts. c.-green LEDs, 3 Watt, E_T = 10 mWatts. d.-red LEDs, 3 Watt, E_T = 16 mWatts

After prolonged reaction times, a secondary photolysis product is observed, consistent with the presence of an unsaturation. This latter product was not isolated neither characterized. At substrate conversion lower than 20 %, only product **2A** is formed. Quantum yield measurements (ϕ), calculation of quenching fractions (Q), and chain lengths (L) for the perfluorobutylation reaction of allyloxybenzene **2** are summarized in Table 6A.

Table 6A. Measurements of quantum yields (ϕ), quenching fractions (Q) and chain lengths (L) for the photoinitiated production of product **2A** from the perfluorobutylation reaction of **2** under three photoinitiated systems

entry	system	ϕ^a	Q^b	L
1	1	1.27 $\pm$ 0.1[c]	0.979	1.3
2	2	2.98 $\pm$ 0.03[d]	0.340	8.8
3	3	0.08 $\pm$ 0.02[e]	0.951	0.09

a.- electronic actinometry employed. Calculation using equation 1. Moles of product formed calculated employing an internal standard by NMR integration (^{19}F and ^{1}H NMR spectroscopy experiments). ϕA = quantum yield for formation of product 2A, ϕ_B = quantum yield for formation of product **2B**. b.-using equation 2, calculation for product **2A**. c.- measured at λ = 392 nm. Photoreaction time 600 sec (see Table S9, ESI). d.- measured at λ = 525 nm. Photoreaction time 1200 sec. (see Table S9, ESI). e.- measured at λ = 657 nm. Photoreaction time 3600 sec. (see Table S9, ESI).

As observed from Table 6A, the chain length for production of product **2A** in the photoinitiated reaction of **2** with n-C_4F_9-I is high for PC-2 (i.e.: 8.8). The production of $^•C_4F_9$ is realized according to Figures 2**A-C**. Then, according to Scheme 3, radicals $^•C_4F_9$ add to the terminal olefinic carbon of substrate **2** to produce intermediate **C** which in turn could abstract an iodine atom from C_4F_9-I to propagate the chain, accounting for the L value obtained with PC-1 and PC-2. The larger reaction quantum yield under PC-2 is a measure of the cumulative efficiency of the process, where a chain propagation as shown in step **II** (Scheme 3**A**) drives the mechanism into an open catalytic cycle. The reaction between excited PC-1* with the additive (i.e.: Cs_2CO_3, step **VII**) is a thermodynamically-favourable or thermoneutral event ($\Delta G_{VII\ (PC^{•-}/\ Cs2CO3)}$ = -0.08 eV, see ESI, section IX.2.). Even more favourable, is the oxidation of radical adduct **C** with PC-1* ($\Delta G_{VII\ (C/\ PC-1*)}$ = - 0.84 V, step **VII**, Scheme 3**B**, see also ESI, section IX.2.) which affords intermediate **D** and PC-1$^{•-}$. Intermediate **D** could suffer iodide nucleophilic attack to render **2A**. Both open catalytic cycles for PC-1 (step **IV**, Scheme 3**B**) and PC-2 (step **II**, Scheme 3**A**) should contribute significantly to the chain propagation as very efficient reaction steps (ATRA reaction).

As stated before, the quenching fractions Q calculated for PC-1 and PC-3 do not directly reflect on the production of $^•C_4F_9$ radicals but the quenching of PC* by additives (step **VII**, Scheme 3**B**, and Stern Volmer plots in Figures S4**A** for PC-1 and S4**C** for PC-3) to afford the reduced forms of PCs (radical anions of PC.-). Consequently, the fractions of the excited photocatalysts (for PC-1*, and PC-3*) that give rise to $^•C_4F_9$ radical production should be smaller than the calculated, depending on the efficiency of process **VII** (Scheme 3**B**). A more realistic fraction of PC* that derives to $^•C_4F_9$ radicals should take into account both processes **VI** and **VII** (Scheme 3**B**). Being process **VI** (i.e.: ΔG_{VI} = +0.38 eV, vide supra[37]) highly inefficient for PC-3, the actual Q' value is expected to be smaller than the calculated (i.e: 0.951) resulting in a larger L. The inefficiency of step **VI** (i.e.: ET reduction of n-C_4F_9-I by PC-3$^{•-}$) translates into a global inefficient

initiation event when using PC-3. In this way, the open catalytic cycle for **2A** production could be activated (vide infra). We surmise that there exists a contribution of an open catalytic cycle responsible for **2A** formation even with PC-3 (step **IV**, Scheme 3**B**) masked by the *Q* and *L* values obtained. Computational data (Table 6B) suggest that radical intermediate **C** (Scheme 3**B**) cannot be oxidized to intermediate **D** by an excited PC-3* as depicted in step **VII**, Scheme 3**B** (entry 2, Table 6B).

Table 6B. Simulated ΔG, ΔH, ΔS at the B3LYP/LANL2DZ theory level at 298 K.

entry	Reaction	ΔG[a]	ΔH[a]	ΔS[a]
1	C₄F₉-I + PCZn·⁻ → ·C₄F₉ + I⁻ + PCZn	-12.11	-3.2	+30
2[b]	(structure)	+17.2	+15.9	-4.5
3[c]	(structure)	-8.1	-9.9	-5.9
4	(structure)	+45.4	+53.5	+27.3

a.-in Kcal/mol. b.-see step VII, Scheme 3B. c.- see step III, Scheme 3A
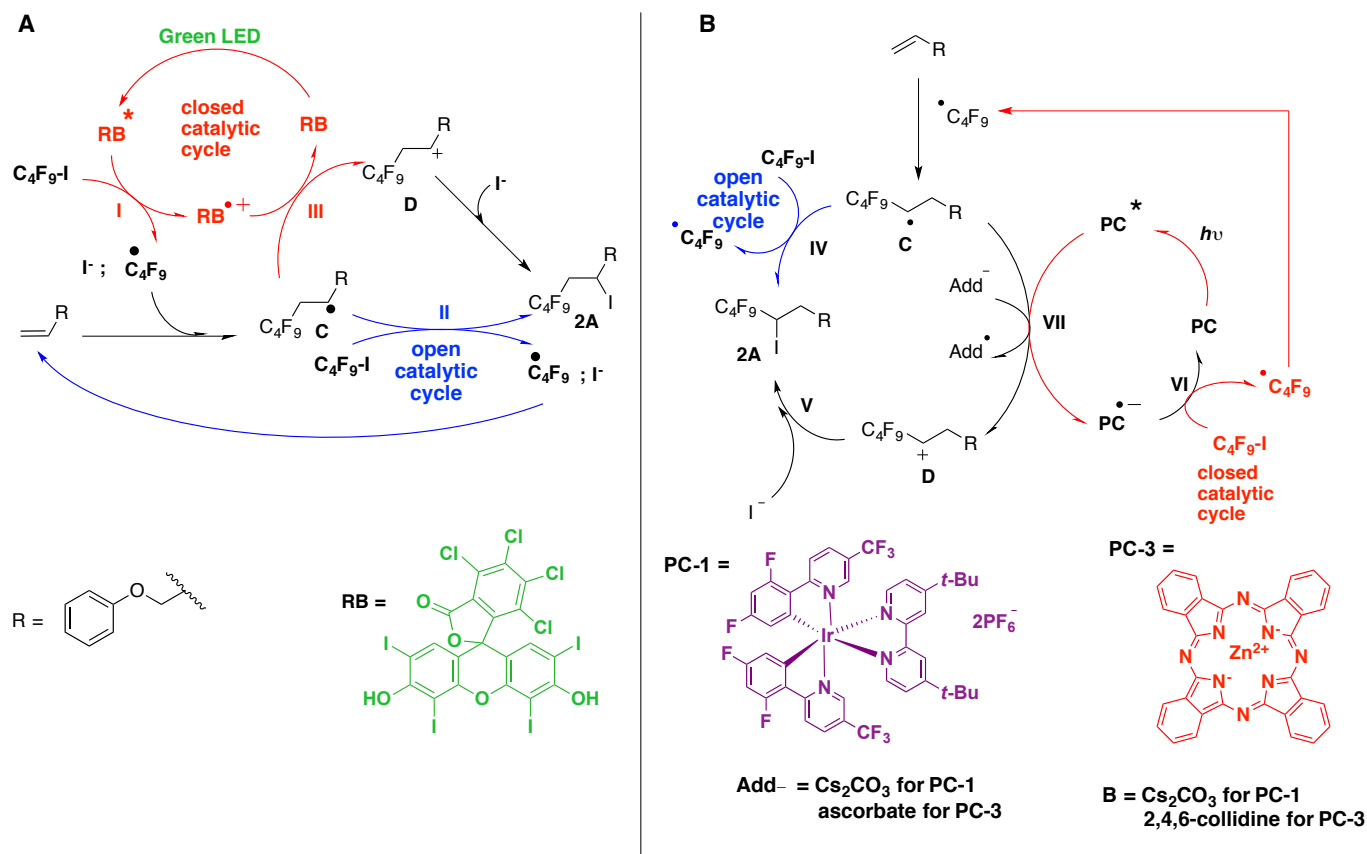
Scheme 3. **A**: Proposed photoinitiated cycle for the perfluorobutylation of allyloxybenzene **2** with PC-2. **B**: idem with PC-1 and PC-3.

In Figure S8 (see ESI), a plot of values of ϕ, *Q*, and *L* for product **2A** under the three photoinitiated systems PC-1-3 is shown, together with oxidation potentials of PC-1-3.

Summary of the photoreaction of allyloxybenzene with ·C₄F₉ radicals

Contrarily to the HAS reaction of **1** with ·C₄F₉ radicals where quantum yields decrease as a function of lowering the photon energy, the quantum yield for the reaction of **2** with ·C₄F₉ radicals is larger for PC-2 than the other two PCs. Postulating the propagation events identical under the three PCs (steps **II** and **IV**, Schemes 3**A** and 3**B**, respectively), we surmise that step **III** with PC-2 (oxidation of radical adduct **C** and regeneration of the active PC-2, Scheme 3**A**) is more efficient than step **VII** (Scheme 3**B**), which means that oxidation of radical adduct **C** by PC·⁺ (step **III**, Scheme 3**A**) to render the carbocation intermediate (which is attacked by iodide anion to give

the final product) is more efficient than the oxidation of **C** by PC-1* or PC-3* (step **VII**, Scheme 3**B**). This latter has been corroborated by calculations, where from Table 6B it is observed that the calculated step **III** (Scheme 3**A**) is an exergonic event by -8.1 Kcal/mol (entry 3, Table 6B), as opposed to highly endergonic process calculated for PC-3 (+ 17.2 Kcal/mol, entry 2, Table 6B). Other termination processes cannot be ruled out at this time, such as those involving the catalysts. One should then postulate in reductive quenching cycles that the major route for generation of the reductive forms of PC-1 and PC-3 (i.e.: PC-1·⁻ and PC-3·⁻) in Scheme 3**B** is the correct choice of the electron donor additive (i.e.: carbonate as in PC-1 and ascorbate for PC-3) rather than ET-oxidation of adduct **C** as in step **VII**.

A lower limit for the chain length of the process could be ca. 9, as observed for PC-2 (Table 6A, entry 2). Also, the nature of the PC influences the chain length, as this should be equal to the actual ratio between the rates of propagation and all termination processes. The fact that the PCs do intervene in termination events (step **III**, Scheme 3**A**, for PC-2, and step **VII**, Scheme 3**B**, for PCs 1 and 3) should bear direct consequence on the length of the chains.

Perfluorobutylation of thiols

The third reaction type investigated was the perfluorobutylation of thiols i.e.: the photoinitiated radical perfluoroalkylation of 2-mercaptoethanol **3**. Table 7 illustrates the yields of the perfluorobutylation product obtained and the mass balance under the three photoinitiated systems. Optimization of reaction conditions is illustrated in ESI.

Table 7. Reaction product from the perfluorobutylation of substrate **3** (0.2 mmol) with n-C$_4$F$_9$-I (3 equiv) employing different photocatalysts PCs (PC-1-3) in indicated Ar-deoxygenated solvent (3 mL), with additives at room temperature for 20 hrs under constant irradiation and stirring.

entry	system	PC (mol%)	$\lambda_{máx}$ (nm)	Mass balance,[a] %
1	1	PC-1 (0.5)	392 [b]	>99
2	2	PC-2 (0.5)	525 [c]	>99
3	3	PC-3 (0.5)	657 [d]	>99

a.- ca. 100% mass balance was obtained, indicating that substrate converts only to product shown. b.-violet LEDs, 3 Watt, E_T = 8 mWatts. c.-green LEDs, 3 Watt, E_T = 10 mWatts. d.-red LEDs, 3 Watt, E_T = 16 mWatts

Quantum yield measurements (ϕ), calculation of quenching fractions (Q) and chain lengths (L) for the perfluorobutylation reaction of 2- mercaptoethanol **3** are summarized in Table 8.

Table 8. Measurements of quantum yields (ϕ), quenching fraction (Q) and chain lengths (L) for the photoinitiated production of product **3A** from the perfluorobutylation reaction of **3** under three photoinitiated systems

entry	system	ϕ^a	Q^b	L^c
1	1	40.7[d] $\pm$ 0.5	0.979	41.6
2	2	228[e] $\pm$ 0.5	0.340	670
3	3	0.34[f] $\pm$ 0.03	0.951	0.36

a.- electronic actinometry employed. Calculation using equation 1. Moles of product formed calculated employing an internal standard by NMR

integration (^{19}F and ^{1}H NMR spectroscopy experiments). b.-using equation 2. c.- $L = \phi / Q$. d.- measured at λ = 392 nm. Irradiation time 150 sec (see ESI). e.- measured at λ = 525 nm. Irradiation time 150 sec. (see ESI). f.- measured at λ = 668 nm. Irradiation time 1200 sec. (see ESI)

The quantum yields observed for the perfluorobutylation reaction of **3** are much higher than unity for PCs-1-2. A large radical chain length (i.e.: 670) is calculated for PC-2, and a significant chain propagation length is encountered for PC-1 (i.e.: 41.6) as well. No chain length is apparent for PC-3.

In Scheme 4**A**, radicals •C$_4$F$_9$ (R$_F$•) are postulated to be produced either through path **II**, or ET reduction from the radical anion of the substitution product (intermediate **C**) to n-C$_4$F$_9$-I (path **IV**, Scheme 4**A**, open catalytic cycle). This latter constitutes an oxidative quenching cycle. In reductive quenching cycles (Scheme 4**B**), radicals •C$_4$F$_9$ are postulated to be produced either from the ET reduction from PC•$^-$ to n-C$_4$F$_9$-I (path **VI**, Scheme 4**B**, closed catalytic cycle) to re-establish thermoneutral PC or ET reduction from the radical anion of the substitution product (intermediate **C**) to n-C$_4$F$_9$-I (path **VII**, Scheme 4**B**, open catalytic cycle). The calculated exergonic nature of both steps **IV** (Scheme 4**A**) and **VII** (Scheme 4**B**) (i.e.: -15.2 Kcal/mol, see ESI, Table S13) accounts for the open catalytic cycle and the large chain lengths observed for PC-1 and PC-2. On the other hand, for PC-3, measured ΔG for step **VI** is very endergonic by +0.38 V.

Quenching fractions Q for PC-1 and PC-3 do not represent directly on the •C$_4$F$_9$ radical production, but the ET reduction of PC-1* and PC-3* by the additive (i.e.: Cs$_2$CO$_3$ for PC-1, Figure S2**A**, and collidinium ascorbate for PC-3, Figure S2**C**) instead; this scenario might be overestimating the actual quenching fraction of PC* that is responsible for •C$_4$F$_9$ radical production. Being process **VI** highly inefficient for PC-3 (Scheme 4**B**), the actual Q' value (which should not only consider step **V** but a combination of **V** and **VI**) is expected to be smaller than the calculated (*i.e*: 0.951) resulting in a larger L. For PCs-1-3, ET from the radical anion of the substitution product **3A**•$^-$ (intermediate C) to n-C$_4$F$_9$-I (paths **IV** and **VII**, Schemes 4**A** and 4**B**, respectively) is likely to play a substantial role in the actual mechanism, generating more •C$_4$F$_9$ radicals and driving the mechanism into an open catalytic cycle.[47]

ARTICLE
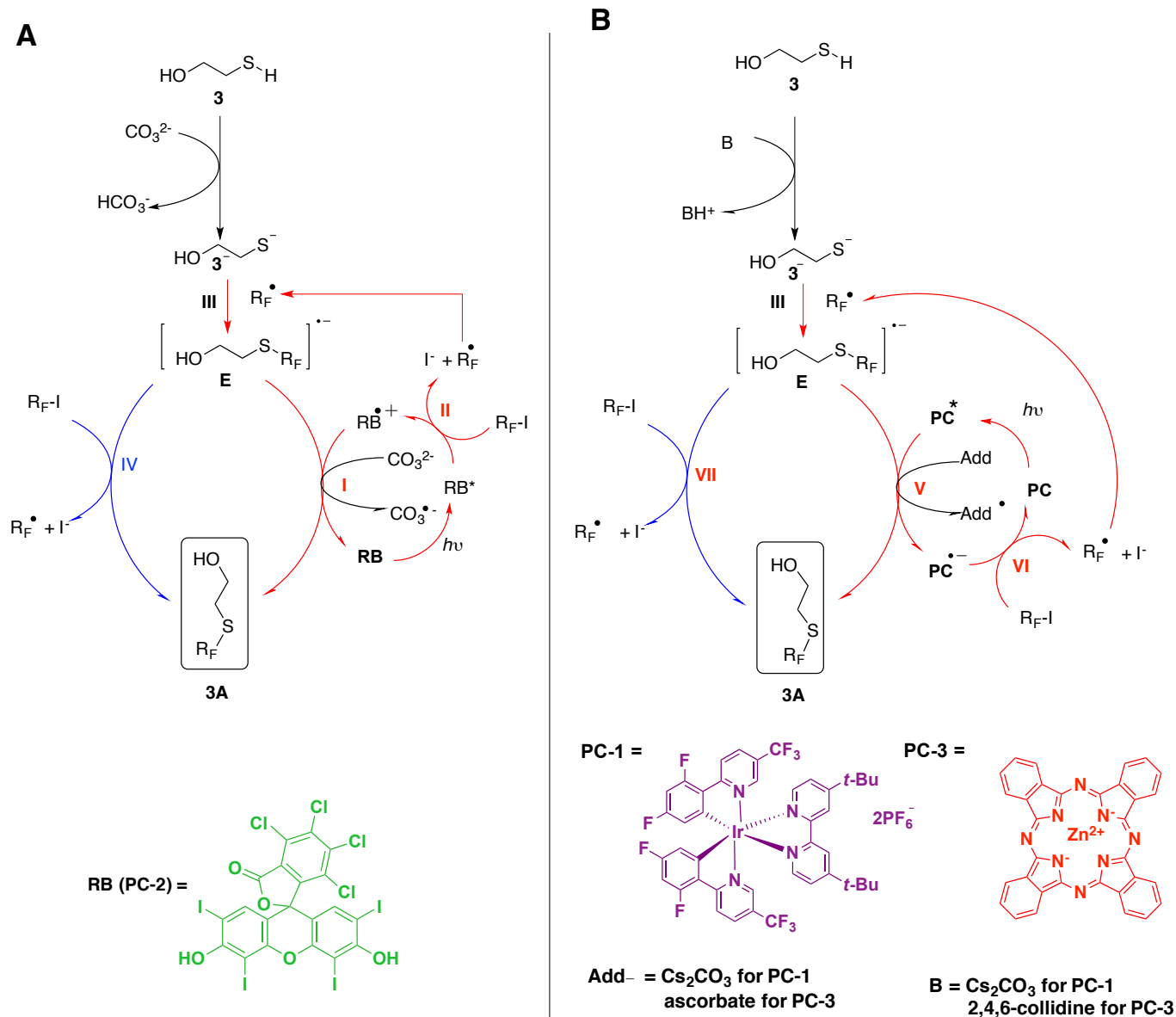
Scheme 4. **A**: Proposed reaction pathway for the perfluoroalkylation of substrate **3** with PC-2. **B**: Proposed reaction pathway for the perfluoroalkylation of substrate **3** with PC-1 and PC-3

Summary of the photoreaction of 2-mercaptoethanol with •C₄F₉ radicals

Being postulated propagation events similar (*c.f.* steps **IV** and **VII**, Schemes 4**A** and 4**B**, respectively) the calculations of chain lengths are biased by the efficiency of the initiation (steps **II** and **VI**, Schemes 4**A** and 4**B**, respectively) and termination (steps **I** and **V**, Schemes 4**A** and 4**B**, respectively). The higher efficiency of the photoreaction with

PC-2, as compared with the other two PCs, might be attributed to a better efficient loop (thermo-neutralization of Rose Bengal radical cation by **E**, step **I**, Scheme 4**A** as opposed to step **V**, Scheme 4**B**, which entails the reduction of excited PC-1* and PC-3*), this latter can be suggested by the redox potentials of RB·⁺/RB and PC*/PC⁻ (+0.74 and +1.02, respectively). As a matter of fact, from theory, it is calculated that step **I**, Scheme 4**A**, is a highly exergonic event by -69 Kcal/mol (Table S13, entry 10), compared to step **V** (Scheme 4**B**)

where the calculated ΔG value for PC-3* is -43 Kcal/mol (Table S13, entry 9).

One could assume that radical chains in the S_{RN} reactions of substrate **3** with •C_4F_9 radicals are significant. The fact that quantum yield under PC-2 is the largest could signify that for the other two PCs (i.e.: PC-1 and PC-3) other inefficient termination events are playing significant roles.

Summary of Quantum yield determinations and chain length calculations

Measurements of quantum yields for the perfluorobutylation reactions of substrates **1-3** with PC-1-3 have been shown in Tables 4, 7, and 8. Table 9 summarizes the quantum yield values for the nine reactions and the chain lengths calculated. In Figure S5 (see ESI), a plot of values of ϕ, Q, and L for products **1-3A** under the three photoinitiated systems PC-1-3 is shown.

Table 9. Quantum yield values and radical chain lengths for the perfluorobutylation of substrates **1-3** under photocatalysts PC-1-3

entry	substrate	PC	K_{SV} (M^{-1})[d]	ϕ[e]	Q	L
1		PC-1[a]	402	3.81 ± 0.16	0.979	3.9
2	1	PC-2[b]	4.3	0.51 ± 0.03	0.340	1.5
3		PC-3[c]	162	0.17 ± 0.01	0.951	0.18
4		PC-1[a]	402	1.27 ± 0.1	0.979	1.3
5	2	PC-2[b]	4.3	2.98 ± 0.03	0.340	8.76
6		PC-3[c]	162	0.08 ± 0.02	0.951	0.09
7		PC-1[a]	402	40.7 ± 0.5	0.979	41.6
8	3	PC-2[b]	4.3	228 ± 5	0.340	670
9		PC-3[c]	162	0.34 ± 0.03	0.951	0.36

a.-violet LEDs, 3 Watt, E_T = 8 mWatts. b.-green LEDs, 3 Watt, E_T = 10 mWatts. c.-red LEDs, 3 Watt, E_T = 16 mWatts. d.-Stern Volmer quenching constant. e.-Quantum yield determined by two parallel methods: electronic actinometry (for PCs-1-3) and potassium ferrioxalate (for PC-1 and PC-2)

Conclusions

Experiments leading to quantum yield measurements and chain length calculations should be considered important mechanistic tools for a variety of reasons.

Although a general conclusion drawn from the nine photoinitiated reactions under the three photocatalytic systems cannot be derived at this time, the denouement of the current study supports conclusions reached by other authors[21] in the sense that quantum yields lower than unity do not necessarily reflect on lack of radical chains, as the global light harvesting efficiency of the photoreaction is distributed among the initiation, propagation and termination steps of the radical chain process. In fact our whole set of reactions are an illustrative example of this scenario. Furthermore a calculated chain length derived from the ratio between the reaction quantum yield and the photocatalyst quenching fraction should not necessarily be taken as the actual chain length or propagation efficiency, as the primary photoinitiation process may not be directly responsible for producing the primary radical initiating species that reacts with the substrate. Also, as chains taken as the ratio of propagation and all terminations steps, these latter vary remarkably within each photocatalyst (for instance see steps **I**

and **VI**, Scheme 2; steps **III** and **VII**, Scheme 3; steps **I** and **V**, Scheme 4). A proper experiment for calculating actual chain lengths would be the employment of the rotating sector experiment where microsecond to second light pulses are employed as discussed by the group of Scaiano for photocatalytic reactions.[21]

Another interesting aspect observed in each set of the studied reactions, is that the photon energy does not necessarily correlate with the quantum yield, since quantum yields are characteristic of photoreactions under a specific set of conditions. In that sense, for the HAS reaction studied, the higher the photon energy the higher the quantum yields, which is not the case in ATRA or S_{RN} reactions studied. This latter is again a consequence of an interplay between the efficiency of the global radical chain photoreaction, that takes into account initiation, propagation and termination cycles. In the case of the ATRA reaction, the higher quantum yield observed for PC-2 is related to the efficiency of propagation and termination processes which outweigh the poorly inefficient initiation event from RB as photocatalyst. This can sometimes counterbalance the use of lower energy irradiation sources in favor of photon efficiency.

For the S_{RN} reaction, the higher photon efficiency observed when using PC-2 can be attributed to the large propagation observed in combination with the efficiency of the step that re-generates the active PC (ET from the radical anion of the substitution product to radical cation of Rose Bengal).

A corollary of the study could be that neither the determination of lower-than-unity quantum yields (equation 2), nor the calculation of chain lengths (as calculated from L) do properly or directly reveal the presence or absence of radical chains in the propagation cycle, especially so if the quenching of the excited state of the PC is not involved in generating the primary radical species.

We show in a concise manner how one could tell the presence of a radical chain length operating in a mechanism of a certain reaction being the quantum yield of the process lower than unity. One way around, which our manuscript shows, would be to study the mechanism with different photocatalysts, that operate under oxidative and reductive quenching manners. This could be useful, specially so for chemists that lack of quantitative methods that can be easily implemented in synthetic laboratories. We suggest that this approach to studying the mechanism of photoinitiated reactions should be generally considered to the growing body of literature involving photoredox catalysis.

Experimental Section
I.-General Considerations

All reactions were carried out in an argon atmosphere under anhydrous conditions. Reaction solvents such as *N,N´*-dimethylformamide (DMF), acetonitrile (MeCN), were chromatography quality and were not further purified. Chromatography and extraction solvents dichloromethane, chloroform, *iso*octane, *n*-hexane, *n*-heptane, ethyl acetate, acetone, dichloromethane (DCM), and ethanol were purchased from commercial suppliers, and distilled before using. Ascorbic acid was 99% pure and used as received from the supplier. 2,4,6-Trimethylcollidine, cesium carbonate (99.99%) and sodium acetate were used as received from the suppliers. Fluorinated reagent 1-iodo-1,1,2,2,3,3,4,4,4-nonafluorobutane (perfluorobutyl iodide), was a commercial reagent and used without further purification. Organic substrates (**1-3**) were vacuum-distilled before use. 2,2,6,6-

Tetramethyl-1-piperidinyloxy (TEMPO), 2-phenylpropene and 1,4-dinitrobenzene were ultra-pure-grade reagents. Dye Rose Bengal (4,5,6,7-tetrachloro-3',6'-dihydroxy-2',4',5',7'-tetraiodo-3*H*-spiro[isobenzofuran-1,9'-xanthen]-3-one), was 99.9% pure and used as received from the supplier. 29*H*,31*H*-phthalocyanine, and the zinc salt of phthalocyanine were commercially available and used as received from the supplier. Photocatalyst 2,9(10),16(17),23(24)-*tetrakis*-(1-adamantylsulfanyl) phthalocyaninatezinc(II), was synthesized according to literature procedures (see section V.-). Photocatalyst [Ir(dF(CF$_3$)ppy)$_2$(dtbbpy))PF$_6$, (dF = 2-(2.4-difluorophenyl)-5-(trifluoromethyl)pyridine, dtbbpy = 4,4´-di-tert-butyl-2,2´-bipyridine) was used as received from the supplier. Zinc acetate was reagent grade. Yields were referred to as isolated yields of analytically pure materials unless otherwise noted, as the case of yields calculated from ^{19}F NMR and ^{1}H NMR spectral integration through the use of internal standard (benzotrifluoride). Reactions for purpose of product isolation (20-h reactions) were magnetically stirred and monitored by thin-layer chromatography (TLC) using Silica gel 60 F254 pre-coated plates (0.25 mm, Merck), and revealed by UV-light. Purification of the reaction products was carried out by column chromatography using Ultra-Pure Silica Gel (230–400 mesh), standard silica-gel for column chromatography (60 mesh) or silica-gel for thin layer preparative chromatography with fluorescent indicator (rhodamine).

The light sources were commercially available high power LEDs (3 Watts): for red light, LED of λ_{max} = 657 nm $\pm$ 2 nm, (radiant power E_T = 16 mWatt; for green light, LED of λ_{max} = 525 nm $\pm$ 2 nm, E_T = 10 mWatt; for violet light, LED of λ_{max} = 392 nm $\pm$ 2 nm, E_T = 8 mWatt). ^{1}H NMR spectra were recorded on a Bruker Avance 500 (500 MHz), or a Bruker Avance 600 (600 MHz) spectrometers, and are reported in ppm using the solvent residual peak resonance as the internal standard (CDCl$_3$ at 7.28 ppm). ^{1}H NMR data are reported as follows: chemical shift; multiplicity; number of hydrogens; coupling constants (Hz). Multiplicity is abbreviated as follows: s = singlet, d = doublet, t = triplet, dd = double doublet, m = multiplet, br = broad, q (quartet), quint (quintet). Proton-decoupled ^{13}C NMR spectra were recorded on a Bruker Avance 500 (at 125.758 MHz), or on a Bruker Avance 600 (at 150.903 MHz) spectrometers and are reported in ppm using the C resonance signal from the solvent as the internal standard (CDCl$_3$ at 77.00 ppm). ^{19}F NMR spectra were recorded on a Bruker Avance 500 (at 470.592 MHz), or a Bruker Avance 600 (at 564.686 MHz) spectrometers and are reported in ppm using the internal standard signal from the spectrometer. High-resolution mass spectra (HRMS) were obtained using JEOL-DX 700 mass spectrometer. UV spectra were recorded on a Jeol double-beam spectrometer.

Separations and purifications were carried out employing silica-gel column chromatography, and the eluants employed are described under compound spectral characterization.

2.-Photocatalytic Reactions

In a 3 mL-reaction vial provided with screw-cap septum and micro stir bar, 0.6 mmol (or 0.2 mmol when noted, as in Table 2) of substrate **1**, **2**, or **3** were introduced. 0.5 mol% of PC-1 (Ir[(dF(CF$_3$)ppy]2(dtbbpy)+), or 5 mol% of PC-2 (Rose Bengal) or 15 mol% of PC-3 (Zinc phthalocyanine) were introduced. Subsequently, 1.5 equiv of additive (Cs$_2$CO$_3$ for PC-1 and PC-2, and ascorbic acid (1.5) collidine (1.5) for PC-3) are placed. Solvent was then introduced (2.5 mL, CH$_3$CN when using PC-1 and PC-2, and a 1 : 1 mixture of CH$_3$CN : DMF for PC-3) were added and the mixture is de-oxygenated with a stream of dry Ar for 15 minutes. After deoxygenation, 3 equivalents of R$_F$-I (*n*-C$_4$F$_9$-I) are then introduced through the septum with microliter syringe. A brief deoxygenation with a slight stream of Ar is passed through for 3 additional minutes. The vessel is placed on a stir plate above the heat dissipator, according to Figures S1-S3. and stirred vigorously for 20 hrs. (at 22 °C) under constant irradiation with high power LED for product isolation, or 60-90 s for quantum yield calculation. After the reaction time elapsed, the mixture was extracted thrice with brine/DCM, and the DCM/DMF extracts evaporated in vacuo. TLC analyses were performed employing dichloromethane:*iso*octane (7 : 3) mobile phase (or otherwise noted). The crude residues were analyzed by ^{1}H NMR, and an ^{19}F NMR integration of the product area is measured. Other runs contain internal standard benzotrifluoride. For isolation purposes, the crude mixture was placed on a silica-gel preparative thin layer glass support and eluted with CHCl$_3$: MeOH or else by column chromatography which was carried out instead of thin layer preparative chromatography. The products reveal intensely under 254 nm-light. The eluants were gathered, evaporated under vacuo, yields calculated by weight and characterized by standard spectroscopic techniques (section VI). NMR integration yields reflect the % of product(s) calculated with the aid of an internal standard (benzotrifluoride for ^{19}F NMR spectra, and 1,3,5-trimethoxybenzene for ^{1} H NMR spectra). For perfluoroalkylthio ether products, a CAN (ceric ammonium nitrate) solution was employed to follow up the reactions by TLC.

3.- Determination of Quantum Yields

This section is fully described in ESI, as section **VII.a.-**

4.-Compound characterization data

This section is fully described in ESI, as section **XI.-** Copies of NMR spectra of all compounds (section **XIII**) and theoretical and thermodynamic calculations (sections **X.1**.- and **X.2**.-) are provided in the ESI.

Computational Simulation Center of CONICET located in Buenos Aires, Argentina.

Conflicts of interest

"There are no conflicts to declare".

Notes and references

1   (a) L. Marzo, S. K. Pagire, O. Reiser, and B. König. *Angew. Chemie* Int. Ed., **2018**, 57, 10034-10072. (b) N. A. Romero and D. A. Nicewicz, *Chem. Rev.*, **2016**, 116, 10075–10166.
2   L. Buzzetti, G. E. M. Crisenza, and P. Melchiorre. *Angew. Chem. Int. Ed.,* **2019**, *58*, 3730 – 3747.
3   R. C. McAtee, E. J. McClain, and C. R. J. Stephenson. *Trends in Chemistry*, **2019**, *1*, 111-125.
4   M. Marchini, G. Bergamini, P. G. Cozzi, P. Ceroni, and V. Balzani. *Angew. Chem. Int. Ed.*, **2017**, *56*, 12820 – 12821.
5   (a) M. S. Lowry, W. R. Hudson, R. A. Pascal and S. Bernhard. *J. Am. Chem. Soc.*, **2004**, *126*, 14129. (b) C. K. Prier, D. A. Rankic and D. W. C. MacMillan. *Chem Rev.*, **2013**, *113*, 5322 (c) A. Singh, K. Teegardin, M. Kelly, K. S. Prasad, S. Krishnan and J. D. Weaver. *J. Organomet. Chem.*, **2015**, *51*, 776. (d) Y. W. Marion, P. H. M. Van Steenburge, C. Barner-Kowollik, M.-F. Reyniers, G. B. Marin, D. R. D`Hooge, *Macromolecules* **2017**, *50*, 1371–1385.
6   (a) M. H. Shaw, J. Twilton, and D. W. C. MacMillan. *J. Org. Chem.*, **2016**, *81*, 6898-6929. (b) J. Twilton, C. Le, P. Zhang, M. H. Shaw, R. W. Evans and D. W. C. MacMillan. *Nat. Chem.*, **2017**, 10.1038/s41570-017-0052.
7   T. C. Sherwood, N. Li, A. N. Yazdani, and T. G. Murali Dhar. *J. Org. Chem.,* **2018**, *83*, 3000–3012.
8   H. S. Han, E. Hye Oh, Y.-S. Jung, and S. B. Han. *Org. Lett.,* **2018**, *20*, 1698-1702.
9   J. Kong, J. Jiang, Y. Huang, Y.-G. Lou, X.-F. Li and C.-Y. He. *Asian J. Org. Chem.*, **2017**, *6*, 1737-1740.
10 P. Chandu, K. G. Ghosh, and D. Sureshkumar. *J. Org. Chem*, **2019**, *84*, 8771-8781.
11 S. J. S. Düsel and B. König. *J. Org. Chem.*, **2018**, *83*, 2802-2807.
12 (a) D. P. Curran. *Synthesis*, **1988**, 417–439; (b) D. P. Curran. *Synthesis*, **1988**, 489–513.
13 M. Majek, F. Filace and A. J. von Wangelin. *Beilstein J. Org. Chem.*, **2014**, *10*, 981–989.
14 K. Matsuzaki, T. Hiromura, E. Tokunaga, and N. Shibata. *ChemistryOpen,* **2017**, *6*, 226 – 230.
15 S. Barata-Vallejo, Sergio M. Bonesi and Al Postigo. *RSC Adv.,* **2015**, *5, 62498-62518*.
16 A. Studer and D. P. Curran. *Nat. Chem.*, **2014**, *6*, 765–773.
17 (a) L. R. Espelt, E. M. Wiensch and T. P. Yoon. *J. Org. Chem.*, **2013**, *78*, 4107–4114. (b) L. R. Espelt, I. S. McPherson, E. M. Wiensch and T. P. Yoon. *J. Am. Chem. Soc.*, **2015**, *137*, 2452–2455.
18 D. Liu, M.-J. Jiao, X.-Z. Wang, and P.-F. Xu. *Org. Lett.*, **2019**, *21*, 4745-4749.
19 (a) M. A. Cismesia and T. P. Yoon. *Chem. Sci.*, **2015**, *6*, 5426. (b) M. Teders, A. Gómez-Suárez, L. Pitzer, M. N. Hopkinson, and F. Glorius. *Angew. Chemie Int. Ed.*, **2017**, *56*, 902-906.
20 (a) G. M. Burnett and H. W. Melville. *Chem. Rev.*, **1954**, *54*, 225–288; (b) R. G. McIntosh, R. L. Eager and J. W. T. Spinks. *Science*, **1960**, *131*, 992; (c) R. G. McIntosh, R. L. Eager and J. W. T. Spinks. *Can. J. Chem.*, **1965**, *43*, 3490–3495.
21 S. P. Pitre, C. D. McTiernan, W. Vine, R. DiPucchio, M. Grenier, and J. C. Scaiano. *Sci Rep.* **2015**, *5*, 16397.
22 (a) A. Dewanji, P. E. Krach, and M. Rueping. *Angew. Chem. Int. Ed.*, **2019,** *58*, 3566 –3570. (b) Q.-Q. Zhou, Y.-Q. Zou, L.-Q. Lu, and W.-J. Xiao. *Angew. Chem. Int. Ed.*, **2019**, *58*, 1586 – 1604.
23 (c) F. Strieth-Kalthoff, M. J. James, M. Teders, L. Pitzer and F. Glorius. *Chem. Soc. Rev.,* **2018**, *47*, 7190-7202.
23 S. Barata-Vallejo, D. E. Yerien, and A. Postigo. *Eur. J. Org. Chem.*, **2015**, 7869–7875.
24 D. E. Yerien, M. V. Cooke, M. C. García Vior, S. Barata-Vallejo and A. Postigo. *Org. Biomol. Chem.*, **2019**, *17*, 3741.
25 See Electronic Supporting Information for Tables optimizations.
26 Q.-Q. Zhou, Y.-Q. Zou, L.-Q. Lu and W.-J. Xiao. *Angew. Chemie Int. Ed.,* **2019**, *58*, 1586-1604.
27 D. W. Clack, N. S. Hush and I. S. Woolsey. *Inorganica Chimica Acta*, **1976**, *19,* 129-132.
28 (a) P. S. Vincett, E. M. Voight and K. E. Rieckhoff. *J. Chem. Phys.*,**1971**, *55*, 4131. (b) A. Harriman, G. Porter and C Richoux. *J. Chem. Soc., Faraday Trans. 2*, **1980**, *75*, 1618-1626.
29 J. Savolainen, D. van der Linden, N. Dijkhuizen and J. L. Herek. *J. Photochem. & Photobiol. A: Chemistry,* **2008**, *196*, 99–105.
30 J. C. del Valle and J. Catalan. *J. Photochem. Photobiol. A: Chem.*, **1993**, *72*, 49-53.
31 M. S. Lowry, J. I. Goldsmith, J. D. Slinker, R. Rohl, R. A. Pascal, Jr., G. G. Malliaras, and S. Bernhard. *Chem. Mater.*, **2005**, *17*, 5712-5719.
32 E. A. Mayeda, L. L. Miller, and J. F. Wolf. *J. Am. Chem. Soc.,* **1972**, *94*, 6812-6816.
33 N. J. W. Straathof, D. J. G. P. van Osch, A. Schouten, X. Wang, J. C. Schouten, V. Hessel and T. Noël. *J. Flow Chem.* **2014**, 4, 12-17.
34 (a) D. E. Yerien, S. Barata-Vallejo, B. Camps, A. E. Cristófalo, M. E. Cano, M. L. Uhrig and A. Postigo. *Catal. Sci. Technol.*, **2017**, *7*, 2274 (b) A. Postigo. *Eur. J. Org. Chem.*, **2018**, 6391-6404.
35 K. Matsuzaki, T. Hiromura, H. Amii and N. Shibata. *Molecules,* **2017***, 22, 1130*.
36 D. A. Armstrong, W. L. Waltz, A. Rauk. *Can. J. Chem.*, **2006**, *84*, 1614–1619.
37 Thermodynamicall unfavourable electron transfer process is also observed see: Y. Shen, J. Cornella, F. Juliá-Hernández and R. Martin. *ACS Catal.*, **2017**, *7*, 409–412.
38 (a) C.-J. Wallentin, J. D. Nguyen, P. Finkbeiner and C. R. J. *J. Am. Chem. Soc.*, **2012**, *134*, 8875–8884; (b) J. D. Nguyen, J. W. Tucker, M. D. Konieczynska and C. R. J. Stephenson. *J. Am. Chem. Soc.*, **2011**, *133*, 4160–4163.
39 R. Beniazza, L. Remisse, D. Jardel, D. Lastécouère and J.-M. Vincent. *Chem. Commun.*, **2018**, *54*, 7451-7454.
40 Y. Wang, J. Wang, G.-X. Li, G. He and G. Chen. *Org. Lett.*, **2017**, *19*, 1442-1445.
41 L. Wozniak, G. Magagnano and P. Melchiorre. *Angew. Chem., Int. Ed.*, **2018**, *57*, 1068-1072.
42 B. Hawthorne, H. Fan-Hagenstein, E. Wood, J. Smith, and T. Hanks. *Int. J. Spectroscopy,* **2013**, *2013, Article ID 216518*.
43 H. J. Kuhn, S. E. Braslavsky, and R. Schmidt. *Pure Appl. Chem.*, **2004**, *76*, 2105–2146.
44 (a) G. H. Searle and G. S. Bull, D. A. House. *J. Chem. Ed.*, **1989**, *66*, 605-608. (b) E. E. Wegner and A. W. Adamson. *J. Am. Chem. Soc.*, **1958**, *80*, 3183.
45 (a) N. J. Turro, Modern Molecular Photochemistry, University Science Books, Sausalito, **1991**. (b) V. Balzani, P. Ceroni and A. Juris, *Photochemistry and Photophysics: Concepts, Research, Applications*, Wiley-VCH, Weinheim, **2014**. (c) L. K. Fraiji, D. M. Hayes, and T. C. Werner. *J. Chem. Ed.* **1992**, *69*, 424-428.
46 D. D. M. Wayner and A. Houmam. *Acta. Chem. Scand*., **1998**, *52*, 377–384.
47 S. Fukuzumi, K. Ohkubo, J. Ortiz, A. M. Gutiérrez, F. Fernández-Lázaro, and Á. Sastre-Santos. *J. Phys. Chem. A,* **2008**, *112*, 10744–10752.
48 (a) E. Magnier, M. Tordeux, R. Goumont, K. Magder and C. Wakselman. *J. Fluorine Chem.*, **2003**, *124*, 55-59. (b) M. Yoshida, M. Ohkoshi, T. Muraoka, H. Matsuyama, and M. Iyoda. *Bull. Chem. Soc. Jpn.*, **2002**, *75*, 1833–1842.
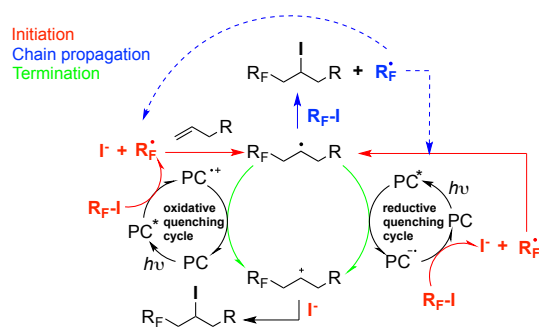
Initiation, propagation and chain termination steps in oxidative and reductive quenching cycles for the photoinitiated perfluoroalkylation reaction of an olefin